J|A|C|S ARTICLES

Published on Web 12/01/2010

Efficient Synthetic Access to Cationic Dendrons and Their Application for ZnO Nanoparticles Surface Functionalization: New Building Blocks for Dye-Sensitized Solar Cells

Jan-Frederik Gnichwitz,[†] Renata Marczak,[‡] Fabian Werner,[§] Nina Lang,[†] Norbert Jux,[†] Dirk M. Guldi,*[,§] Wolfgang Peukert,*[,‡] and Andreas Hirsch*[,†]

Department of Chemistry and Pharmacy & Interdisciplinary Center of Molecular Materials (ICMM), Friedrich-Alexander-University Erlangen-Nuremberg, Henkestrasse 42, 91054 Erlangen, Germany, Institute of Particle Technology, Friedrich-Alexander-University Erlangen-Nuremberg, Cauerstrasse 4, 91058 Erlangen, Germany, and Department of Chemistry and Pharmacy & Interdisciplinary Center of Molecular Materials (ICMM), Friedrich-Alexander-University Erlangen-Nuremberg, Egerlandstrasse 3, 91058 Erlangen, Germany

Received July 9, 2010; E-mail: w.peukert@lfg.uni-erlangen.de; guldi@chemie.uni-erlangen.de; andreas.hirsch@chemie.uni-erlangen.de

Abstract: A new concept for the efficient synthesis of cationic dendrons, 4-*tert*-butyl-1-(3-(3,4-dihydroxybenzamido)benzyl)pyridinium bromide (**17**), 1,1′-(5-(3,4-dihydroxybenzamido)-1,3-phenylene)bis(methylene)bis(4-*tert*-butylpyridinium) bromide (**18**), *N*1,*N*7-bis(3-(4-*tert*-butyl-pyridium-methyl)phenyl)-4-(3-(3-(4-*tert*-butyl-pyridinium-methyl)phenyl-amino)-3-oxopropyl)-4-(3,4-dihydroxybenzamido)heptanediamide tribromide (**19**), and *N*1,*N*7-bis(3,5-bis(4-*tert*-butyl-pyridium-methyl)phenyl)-4-(3-(3,5-bis(4-*tert*-butyl-pyridinium-methyl)phenylamino)-3-oxopropyl)-4-(3,4-dihydroxybenzamido)heptanediamide hexabromide (**20**), and their facile binding to zinc oxide (ZnO) nanostructures is introduced. Dendrons containing highly reactive benzylic bromides reacted readily with 4-*tert*-butyl-pyridine and resulted in cationic dendrons. Furthermore, these permanently positively charged dendrons were equipped with a catechol anchor group. This enabled ZnO surface functionalization by simple immersion. The adsorption of **17**, **18**, **19**, and **20** on the colloidal nanoparticles was monitored by Langmuir isotherms. The highest obtained experimental loadings correspond to 99.5%, 98.6%, 99.1%, and 42.5% of the particle surface for **17**, **18**, **19**, and **20**, respectively. These results indicate insufficient adsorption of the largest molecule **20** leading to reduced colloidal stability of the nanoparticles, while an enhanced stability after grafting with **17**, **18**, and **19** was observed. Mesoporous films suitable for the use as electrodes in dye-sensitized solar cells (DSSCs) were prepared. Subsequently, the films were functionalized with **18**, **19**, or **20** and sensitized with zinc-5,15-bis-[2′,6′-bis-{2″,2″-bis-(carboxy)-ethyl}-methyl-4′-*tert*-butyl-pheny]-10,20-bis-(4′-tert-butylphenyl)porphyrin-octasodium-salt. UV−vis absorption spectra confirmed that **18**, **19**, and **20** are suitable for the stable electrostatic attachment of the dye. Current−voltage characteristics of complete cells demonstrated that increasing positive functionalization of the ZnO surface leads to decreased open circuit voltages (V_{oc}). All V_{oc} values were around 0.4 V with a maximum for the **18** functionalized ZnO film of 0.45 V. The maximum cell efficiency obtained (0.31%) is rather high, considering the narrow spectral absorption of the dye and the rather thin ZnO films used. Finally, incident photon to current efficiency (IPCE) measurements confirmed photoinduced electron injection from the dye. These features are important assets for applications in particle technology and even facilitated advanced devices like a supramolecular DSSC complete with a subsequent layer of negatively charged porphyrins.

Introduction

Coulomb interactions are rather fundamental noncovalent binding motifs in nature, where they play an important role as key interactions, for example, in biological macromolecules such as enzymes and DNA. Recently, supramolecular organization of charged artificial polymers using noncovalent Coulomb interactions has emerged as a very powerful construction principle for novel hierarchically ordered molecular materials with unprecedented mechanical[1,2] and electronic[3−5] properties. As an example of this approach, we have recently reported the

[†] Department of Chemistry and Pharmacy & Interdisciplinary Center of Molecular Materials (ICMM), Friedrich-Alexander-University Erlangen-Nuremberg, Henkestrasse 42.

[‡] Institute of Particle Technology, Friedrich-Alexander-University Erlangen-Nuremberg.

[§] Department of Chemistry and Pharmacy & Interdisciplinary Center of Molecular Materials (ICMM), Friedrich-Alexander-University Erlangen-Nuremberg, Egerlandstrasse 3.

(1) Decher, G. *Science* **1997**, *277*, 1232.
(2) Kaschak, D. M.; Lean, J. T.; Waraksa, C. C.; Saupe, G. B.; Usami, H.; Mallouk, T. E. *J. Am. Chem. Soc.* **1999**, *121*, 3435.
(3) Pitigala, P. K. D. D. P.; Seneviratne, M. K. I.; Perera, V. P. S.; Tennakone, K. *Langmuir* **2004**, *20*, 5100.
(4) Carlisle, J. R.; Weck, M. *Funct. Org. Mater.* **2007**, 261.

 10.1021/ja106076h

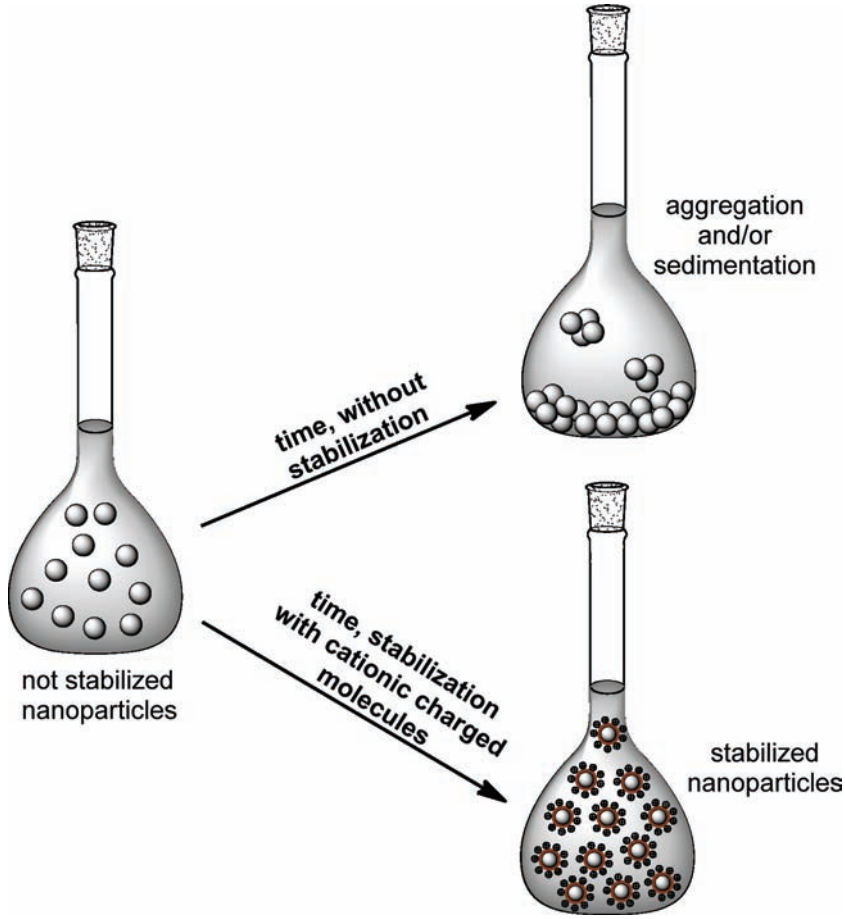

Figure 1. Dispersion of unfunctionalized nanoparticles without stabilization (on the top) resulting in sedimentation and stabilized nanoparticles functionalized with charged dendrons (on the bottom) resulting in a very stable suspension.

strong interaction between oppositely charged fullerenes and porphyrins/cytochrome *c*.[6] In fact, the resulting hybrid structures possess sufficiently strong electronic coupling between their constituent components to permit internal charge separation processes to occur. In another contribution, the interplay of electrostatic attractions and repulsions was used as the modus operandi between charged polyions to form self-assembled multilayers, where the assembly and degradation behavior were tested.[7] Moreover, we have also reported on the strong binding between metalloporphyrins equipped with catechol anchoring groups and zinc oxide (ZnO) nanoparticles used for the construction of dye-sensitized solar cells (DSSCs).[8] Because of its direct bandgap as well as excellent thermal, chemical, and structural features, ZnO has emerged as a fascinating material for a broad range of electronic, optical, and piezoelectric applications. In particular, recent interest in ZnO has focused on its application in light emitting diodes,[9] transparent electrodes,[10,11] sensors,[12] and photovoltaics.[13−18]

The successful utilization of nanoparticles is often limited by their tendency to aggregate, a feature that stems from their high surface area-to-volume ratio. The improvement of stability can directly influence the ability of nanoparticles to form densely packed layers (Figure 1), a morphology essential to the successful operation of, for example, thin-film transistors,[19,20]

(5) Ponader, S.; Rosenlehner, K.; Vairaktaris, E.; von Wilmowsky, C.; Schlegel, K.; Neukam, F.; Schmidt, C.; Schunk, T.; Hirsch, A.; Nkenke, E. *J. Mater. Sci.: Mater. Med.* **2009**, *20*, 2455.
(6) Guldi, D. M.; Zilbermann, I.; Anderson, G.; Li, A.; Balbinot, D.; Jux, N.; Hatzimarinaki, M.; Hirsch, A.; Prato, M. *Chem. Commun.* **2004**, 726.
(7) Rosenlehner, K.; Schunk, T.; Jux, N.; Brettreich, M.; Hirsch, A. *Org. Biomol. Chem.* **2008**, *6*, 2697.
(8) Marczak, R.; Werner, F.; Gnichwitz, J.-F.; Hirsch, A.; Guldi, D. M.; Peukert, W. *J. Phys. Chem. C* **2009**, *113*, 4669.
(9) Colvin, V. L.; Schlamp, M. C.; Alivisatos, A. P. *Nature* **1994**, *370*, 354.
(10) Durán, P.; Capel, F.; Tartaj, J.; Moure, C. *Adv. Mater.* **2002**, *14*, 137.
(11) Yang, M.; Wang, D.; Peng, L.; Zhao, Q.; Lin, Y.; Wei, X. *Sens. Actuators, B* **2006**, *117*, 80.
(12) Rout, C. S.; Raju, A. R.; Govindaraj, A.; Rao, C. N. R. *Solid State Commun.* **2006**, *138*, 136.
(13) Grätzel, M. *J. Photochem. Photobiol., C: Photochem. Rev.* **2003**, *4*, 145.
(14) O'Regan, B.; Gratzel, M. *Nature* **1991**, *353*, 737.
(15) Quintana, M.; Edvinsson, T.; Hagfeldt, A.; Boschloo, G. *J. Phys. Chem. C* **2006**, *111*, 1035.
(16) Redmond, G.; Fitzmaurice, D.; Graetzel, M. *Chem. Mater.* **1994**, *6*, 686.
(17) Zeng, L.; Dai, S.; Xu, W.; Wang, K. *Plasma Sci. Technol.* **2006**, *8*, 172.
(18) Werner, F.; Gnichwitz, J.-F.; Marczak, R.; Palomares, E.; Peukert, W.; Hirsch, A.; Guldi, D. M. *J. Phys. Chem. B* **2010**, *114*, 14671.
(19) Walther, S.; Schäfer, S.; Jank, M. P. M.; Thiem, H.; Peukert, W.; Frey, L.; Ryssel, H. *Microelectron. Eng.* **2010**, *87*, 2312.
(20) Sun, B.; Sirringhaus, H. *Nano Lett.* **2005**, *5*, 2408.

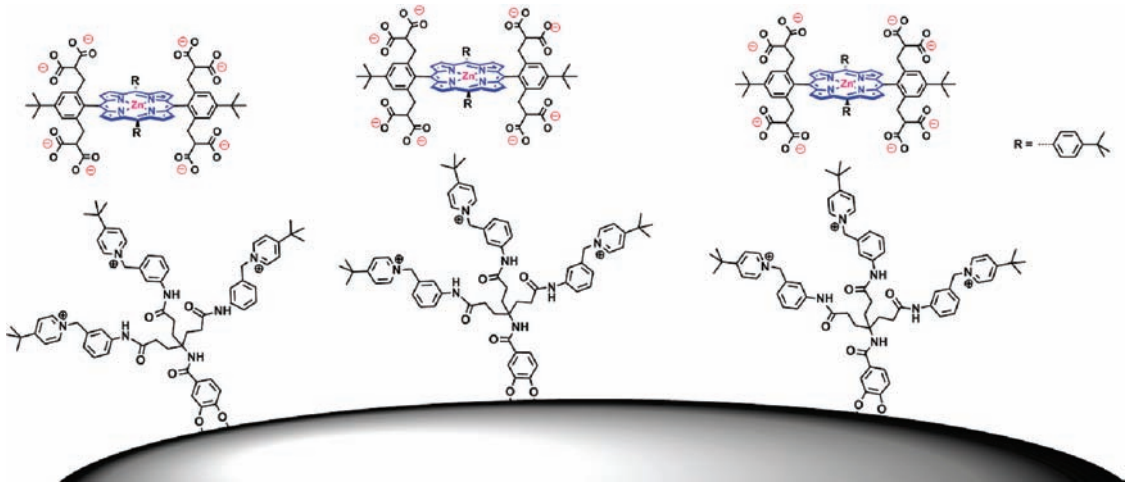

Figure 2. Illustration of electrostatic interaction between the negatively charged dye **21** [2′,6′-bis-{2″,2″-bis-(carboxy)-ethyl}-methyl-4′-*tert*-butyl-pheny]-10,20-bis-(4′-*tert*-butylphenyl)porphyrin-octasodium-salt and the ZnO surface modified with positively charged dendron **18** in the supramolecular dye-sensitized solar cell.

transparent conductive films,[21,22] or solar cells.[3,23] Various strategies exist that impart colloidal stability on nanoparticles and that rely mainly on the provision of electrostatic or steric repulsions between the particles.[24,25] A highly effective combination of these effects, often referred to as electrosteric stabilization, can be achieved by modifying the surface of nanoparticles with ionic surfactants, charged oligomers, or polyelectrolytes. This procedure may lead to an increase, decrease, or even inversion of the apparent particle surface charge, while the conformational entropy of the adsorbate provides additional protection against aggregation. Besides improving the colloidal stability, the modification of solid surfaces by such charged moieties is of high technological significance because the electrostatic interaction allows differently functionalized particles to behave as self-assembling "building blocks".

There are two general approaches for attaching charged molecules, oligomers, or macromolecules to particle surfaces. First, polyelectrolytes can be bound physically (physisorption) utilizing the inherent, but often pH dependent, surface charge of the substrate[26−31] or following its charge-inducing etching.[32] One drawback of this approach is that the stability of the physisorbed layer can be strongly influenced by the environment, that is, solvents and pH, and desorption of the layer may even occur.[33,34] The second general method for surface modification circumvents this by anchoring the absorbate through the formation of covalent bonds with the substrate (chemisorption).[35−37] One issue that still remains, however, is that the degree of charging depends on the pH, which may limit the effectiveness of the functionalized particle to form self-assembled structures. It is therefore a particular challenge to the synthetic community to produce chemisorbing moieties that possess pH-independent permanent charges.

In the present work, we report the synthesis of cationic dendrons, which can be readily anchored to ZnO nanoparticles via a catechol group and which possess dendrons with a pH-independent charge. This approach leads to the formation of more homogenously coated particles and surfaces than methods where chemical post treatments are performed after the grafting of precursors.[35−37] Our cationic dendrons provide not only an excellent colloidal stability to the particulate systems, but also a modified ZnO surface, which is suitable for assembling with oppositely charged entities in a layer-by-layer fashion.[1] We demonstrate this possibility by assembling an anionic dye molecule onto films of the cationic functionalized ZnO nanoparticles and applying the structure as a photoanode in a dye-sensitized solar cell (Figure 2). We believe that this is the first example of a sensitizer being attached to the inorganic host in such a fashion. We observe that the approach is successful due to the built-in driving force for electrons to be drawn to the metal oxide surface, given by the positive charges attached between the acceptor (ZnO) and the dye.

Results and Discussion

Syntheses of the Cationic Dendrons. Only few examples are known in which permanent cationic charges are included in functional molecules or dendrimers. These include the reaction of tertiary amines with halogenides,[38−42] the substitution of primary

(21) Reindl, A.; Mahajeri, M.; Hanft, J.; Peukert, W. *Thin Solid Films* **2009**, *517*, 1624.
(22) Mahajeri, M.; Voigt, M.; Klupp Taylor, R. N.; Reindl, A.; Peukert, W. *Thin Solid Films* **2010**, *518*, 3373.
(23) Guldi, D. M.; Rahman, G. M. A.; Sgobba, V.; Kotov, N. A.; Bonifazi, D.; Prato, M. *J. Am. Chem. Soc.* **2006**, *128*, 2315.
(24) Derjaguin, B. V.; Landau, L. D. *Acta Physicochimica URSS* **1941**, *14*, 633.
(25) Verwey, E. J. W.; Overbeek, T. G. *Theory of the Stability of Lyophobic Colloids*; Elsevier: Amsterdam, 1948.
(26) Decher, G.; Hong, J. D.; Schmitt, J. *Thin Solid Films* **1992**, *210−211*, 831.
(27) Fendler, J. H.; Meldrum, F. C. *Adv. Mater.* **1995**, *7*, 607.
(28) Gao, M.; Richter, B.; Kirstein, S.; Mohwald, H. *J. Phys. Chem. B* **1998**, *102*, 4096.
(29) Pastoriza-Santos, I.; Koktysh, D. S.; Mamedov, A. A.; Giersig, M.; Kotov, N. A.; Liz-Marzán, L. M. *Langmuir* **2000**, *16*, 2731.
(30) Ariga, K.; Hill, J. P.; Ji, Q. *Phys. Chem. Chem. Phys.* **2007**, *9*, 2319.
(31) Vaccaro, A.; Hierrezuelo, J.; Skarba, M.; Galletto, P.; Kleimann, J. R.; Borkovec, M. *Langmuir* **2009**, *25*, 4864.
(32) Fujita, S.; Shiratori, S. *Nanotechnology* **2005**, *16*, 1821.
(33) Ramachandran, R.; Somasundaran, P. *J. Colloid Interface Sci.* **1987**, *120*, 184.
(34) Tanaka, H.; Ödberg, L.; Wågberg, L.; Lindström, T. *J. Colloid Interface Sci.* **1990**, *134*, 229.
(35) Mir, Y.; Auroy, P.; Auvray, L. *Phys. Rev. Lett.* **1995**, *75*, 2863.
(36) Biesalski, M.; Ruhe, J. *Macromolecules* **1999**, *32*, 2309.
(37) Zhang, H.; Ruhe, J. *Macromolecules* **2003**, *36*, 6593.
(38) Chen, C. Z.; Beck-Tan, N. C.; Dhurjati, P.; van Dyk, T. K.; LaRossa, R. A.; Cooper, S. L. *Biomacromolecules* **2000**, *1*, 473.

Scheme 1. (A) Stoddard's Prototype of a Polycationic Dendrimer Obtained via a Substitution of Benzylic Bromides with Tertiary Amines and Subsequent Counter Ion Exchange; (B) Cationic Charged Porphyrin of Jux Synthesized by a Condensation Reaction of a Benzaldehyde with Benzylic Methylether Groups in the Ortho Position, Which Are Replaced by Benzylic Bromides with HBr/Acetic Acid and Subsequently Substituted with *tert*-Butylpyridine, Leading to an Octa-cationic Porphyrin

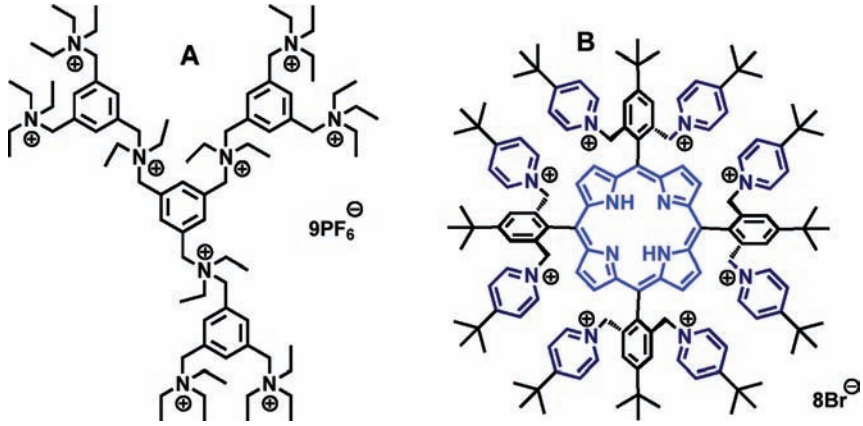

bromide by pyridine,[43,44] or the alkylation of polypyridines.[45,46] Stoddart et al. published in 1997 a new method to synthesize polycationic dendrimers[47] by using benzylic bromides as a substitution center. These highly reactive centers react with tertiary amines nearly quantitatively to yield architectures decorated with numerous cationic charges. Jux modified this method by employing a methoxyether-substituted benzaldehyde for the synthesis of porphyrins, Scheme 1.[48] The methoxyether protecting groups preserve the reactivity of the benzylic bromide during subsequent reaction steps. Acidic conditions using hydrogen bromide in glacial acetic acid were selected to perform the quantitative deprotection to yield the corresponding benzylic bromide. The final replacement was performed with numerous nucleophiles. Among the latter, pyridine is of great importance, because its use results in a quarternized nitrogen center and a cationic charge balanced by bromide. The high reactivity of the benzylic bromides due to their preference for substitution reactions in the benzylic position as well as the nearly quantitative conversion of the benzylic methoxyether to the benzylic bromide inspired us to develop a system that displays these features and can easily be used for the addition of extra functionalities.

Our synthesis started from 3-(methoxymethyl)aniline (**1**). As described in the literature,[49] 1-(chloromethyl)-3-nitrobenzene was treated with sodiummethanolate to obtain 1-(methoxymethyl)-3-nitrobenzene in very good yields (83%). The reduction

Scheme 2. Synthesis of the Two Main Building Blocks, 3-(Methoxymethyl)aniline (on the Top, **1**) and 3,5-Bis(methoxymethyl)aniline (on the Bottom, **2**)

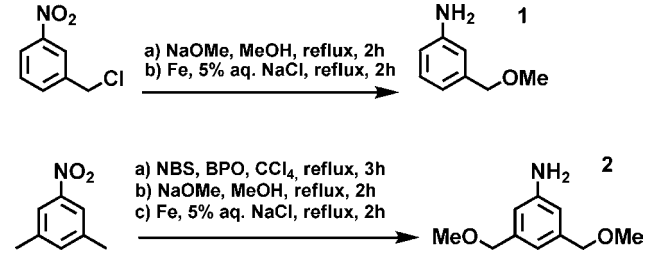

to the corresponding aniline derivative was performed by means of iron in an aqueous solution of sodium chloride. The desired product was obtained in 55% yield without appreciable amounts of any byproduct. Thus, the syntheses of 3-(methoxymethyl)aniline and 3,5-bis(methoxymethyl)aniline (**2**) were successfully carried out. Here, the reaction starts from 1,3-dimethyl-5-nitrobenzene, which was treated with *N*-bromosuccinimide (NBS) and dibenzoyl peroxide (DBPO) in refluxing carbontetrachloride to obtain 1,3-bis(bromomethyl)-5-nitrobenzene.[50] Light-induced bromination of the nitro-xylene leads mainly to the monobrominated product, whereas the bromination with NBS afforded the target compound in 20% yield. To avoid oligomeric products, the benzylic bromide was transformed into ether moieties prior to the reduction of the nitro-group. In this regard, the ether synthesis was accomplished by using sodiummethanolate, which yielded 1,3-bis(methoxymethyl)-5-nitrobenzene. The final reduction to 3,5-bis(methoxymethyl)aniline (**2**) was carried out in the same conditions as the procedure for 3-(methoxymethyl)aniline, Scheme 2.

The two main building blocks (**1** and **2**) are versatile precursors to control the number of charges. The connection between the aniline-derivatives and the compound to be functionalized should preferably be an amide bond for stability reasons. Thus, modified Steglich conditions[51,52] with 1-(3-dimethylaminopropyl)-3-ethylcarbodiimide hydrochloride (EDC) and 1-hydroxybenzotriazole (HOBT) as coupling agents are used. Because of the decreasing yields in multiple coupling reactions, we decided to develop a dendrimer containing

(39) Schlapak, R.; Armitage, D.; Saucedo-Zeni, N.; Latini, G.; Gruber, H. J.; Mesquida, P.; Samotskaya, Y.; Hohage, M.; Cacialli, F.; Howorka, S. *Langmuir* **2007**, *23*, 8916.
(40) Almarsson, O.; Adalsteinsson, H.; Bruice, T. C. *J. Am. Chem. Soc.* **1995**, *117*, 4524.
(41) Virboul, M. A. N.; Lutz, M.; Siegler, M. A.; Spek, A. L.; van Koten, G.; Klein Gebbink, R. J. M. *Chem.-Eur. J.* **2009**, *15*, 9981.
(42) Plault, L.; Hauseler, A.; Nlate, S.; Astruc, D.; Ruiz, J.; Gatard, S.; Neumann, R. *Angew. Chem., Int. Ed.* **2004**, *43*, 2924.
(43) Liu, G.-F.; Filipovi, M.; Ivanovi, I.; Beuerle, F.; Witte, P.; Hirsch, A. *Angew. Chem., Int. Ed.* **2008**, *47*, 3991.
(44) Kuhnen-Clausen, D.; Hagedorn, I.; Bill, R. *J. Med. Chem.* **1979**, *22*, 177.
(45) Shifrina, Z. B.; Kuchkina, N. V.; Rutkevich, P. N.; Vlasik, T. N.; Sushko, A. D.; Izumrudov, V. A. *Macromolecules* **2009**, *42*, 9548.
(46) Miskelly, G. M.; Webley, W. S.; Clark, C. R.; Buckingham, D. A. *Inorg. Chem.* **1988**, *27*, 3773.
(47) Stoddart, J. F.; Ashton, P. R.; Shibata, K.; Shipway, A. N. *Angew. Chem., Int. Ed. Engl.* **1997**, *36*, 2781.
(48) Jux, N. *Org. Lett.* **2000**, *2*, 2129.
(49) Wan, P.; Muralidharan, S.; McAuley, I.; Babbage, C. A. *Can. J. Chem.* **1987**, *65*, 1775.
(50) In, S.; Cho, S. J.; Lee, K. H.; Kang, J. *Org. Lett.* **2005**, *7*, 3993.
(51) Hoefle, G.; Steglich, W. *Chem. Ber.* **1972**, *105*, 1368.
(52) Neises, B.; Steglich, W. *Angew. Chem.* **1978**, *90*, 556.

Scheme 3. Two Possible Ways To Synthesize the Dendrimers **7** and **8**

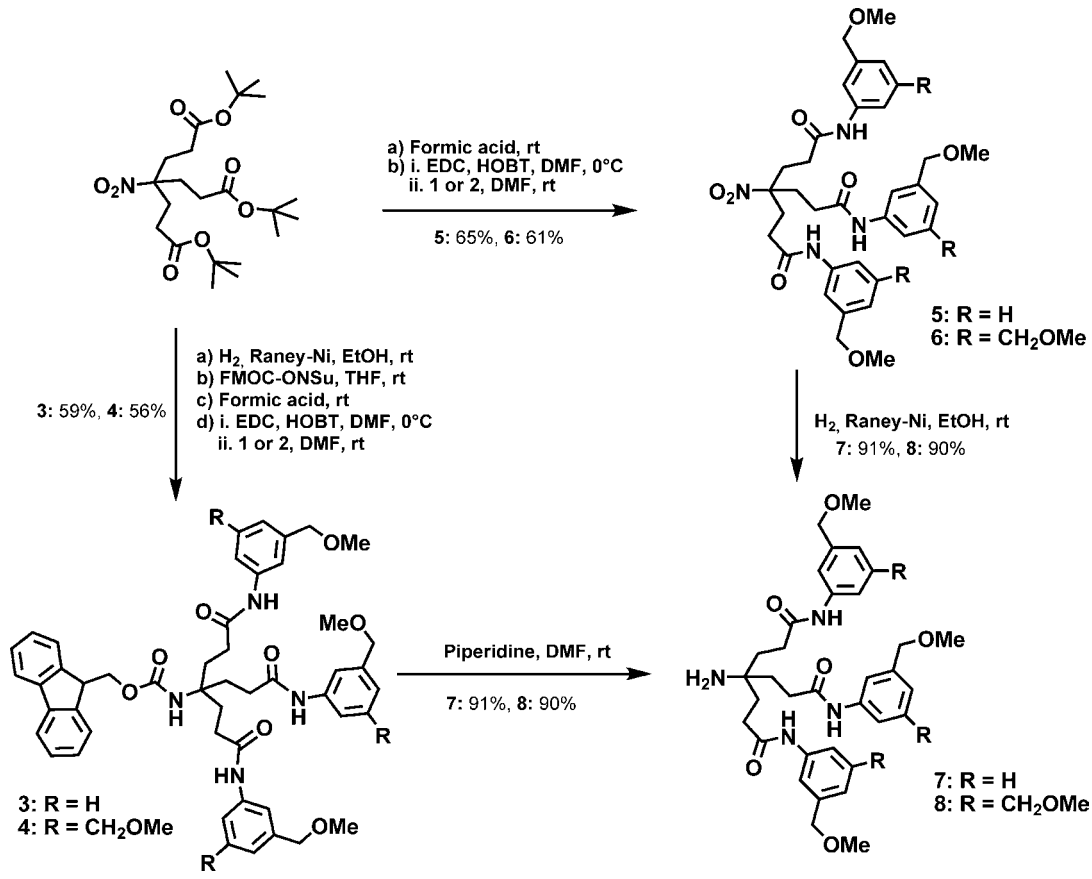

the building blocks **1** and **2**, which can multiply the amount of charges with just one reaction. A useful dendrimer[53] for this purpose is the deprotected first generation Newkome-Dendrimer[54−56] because it possesses three carboxylic acids that cannot only be utilized in basic media for negative charges but also for further reactions. The focal nitro-group can be reduced in a final reaction step and provides a new functional group for further functionalization. We synthesized the target dendrimers **7** and **8** in two different ways (Scheme 3). In one case, the reduction of the nitro group was done first, followed by its protection with *N*-(9*H*-fluoren-2-ylmethoxycarbonyloxy)succinimide (FMOC-ONSu). The *tert*-butylester was cleaved with formic acid followed by a 3-fold amide coupling with the corresponding aniline **1** or **2**. Finally, the fmoc protecting group was removed by basic treatment with pyridine to obtain the desired compounds **7** and **8**. The other route leads first to the 3-fold amide coupling after acidic deprotection followed by reduction of the focal nitro-group to the corresponding target dendrimers. This route is two steps shorter than that aforementioned, and the overall yields (54% and 50% in comparison to 59% and 55%) are only a little lower. The amines **7** and **8** are not stable over longer periods of time, so that they have to be kept cold and stored in the dark.

3,4-Diphenylmethylenedioxyprotocatechuic acid[57] was reacted with the amines **1**, **2**, **7**, and **8** to obtain the intermediates **9**, **10**, **11**, and **12**, respectively (Scheme 4). Thereby, one anchoring group can bear one, two, three, or six charges per molecule, which allows control of the amount of charges on the surface when these molecules are combined with dispersed nanoparticles or surfaces of films. The dihydroxy functionality of the catechol has to be protected because at least one purification step via column chromatography on silica is needed. Besides the high affinity of the catechol to ZnO- or TiO_2-surfaces, the attachment to SiO_2 is also very strong, so that purification of the reaction mixture via column chromatography with silica leads to a high loss of product, which was avoided conveniently via this protection step.

The diphenylmethane protecting group can be removed easily with formic acid resulting in quantitative yields. Interestingly, as the benzylic methyl ether is cleaved by treatment with hydrobromic acid in glacial acetic acid, the deprotection of the catechol unit and the generation of the benzylic bromide can be achieved in one step. Both transformations are quantitative including a simple workup. The benzylic bromides of the resulting compounds **13**, **14, 15**, and **16** are very reactive. THF was chosen for the quaternization of **13** and **14**, but in the case of **15** and **16** partly quarternized compounds precipitated preventing complete conversion. In contrast, partially and fully charged compounds remain dissolved in DMF, so that all target cationic compounds **17**, **18**, **19**, and **20** were accessible (Scheme 5 and Table 1).

(53) Astruc, D.; Boisselier, E.; Ornelas, C. T. *Chem. Rev.* **2010**, *110*, 1857.
(54) Newkome, G. R.; Behera, R. K.; Moorefield, C. N.; Baker, G. R. *J. Org. Chem.* **1991**, *56*, 7162.
(55) Newkome, G. R.; Nayak, A.; Behera, R. K.; Moorefield, C. N.; Baker, G. R. *J. Org. Chem.* **1992**, *57*, 358.
(56) Brettreich, M.; Hirsch, A. *Synlett* **1998**, 1396.
(57) Iacazio, G.; Périssol, C.; Faure, B. *J. Microbiol. Methods* **2000**, *42*, 209.

Scheme 4. Synthesis of the Intermediates **9**, **10**, **11**, and **12** via Modified Steglich Coupling Reaction

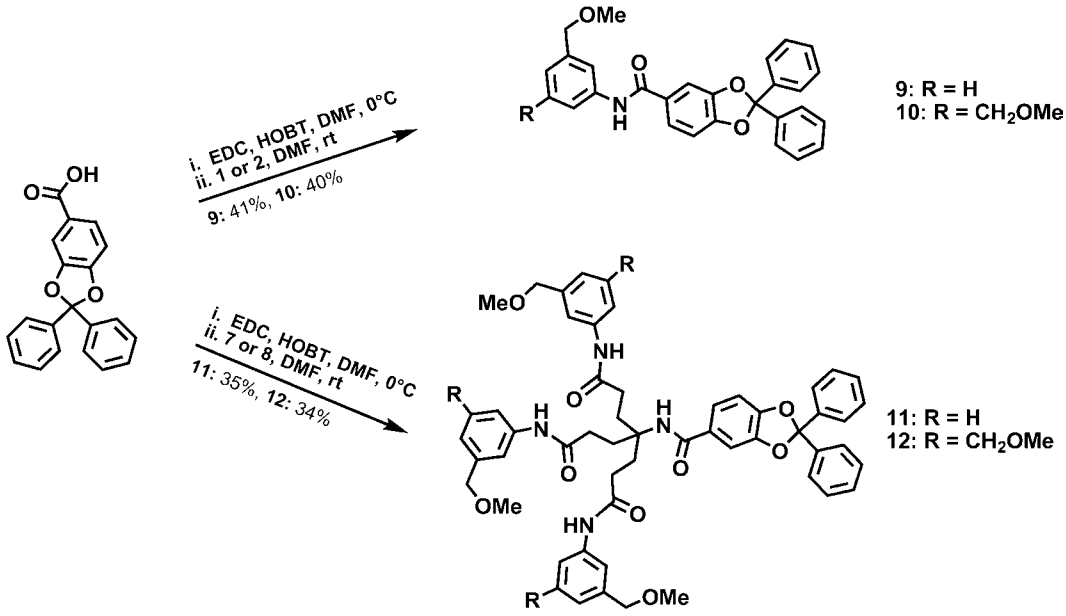

The progress of the quaternization can be followed easily via ^{1}H NMR spectroscopy. The signal of the protons of the benzylic methylene group shifts upon substitution with the pyridine unit to 5.8 ppm. Thus, if the signal at 4.5 ppm corresponding to the protons of the benzylic bromide has completely vanished, a full conversion is achieved.

ZnO Quantum Dot Synthesis and Functionalization. The adsorption of polyelectrolytes on oxide nanoparticles and its application in preparing colloidal dispersions have been the subjects of intensive theoretical and experimental studies. For example, coating of polymers such as poly(methyl methacrylate) (PMMA), poly(styrene) (PSt), poly(ethylene glycol) (PEG), or poly(acrylic acid) (PAA) on the surface of ZnO nanoparticles has been widely investigated.[58−62] However, many chemical steps are required during the adsorption procedure. Moreover, this approach provides only limited control over the thickness and homogeneity of the attached polymers. Therefore, the present study is focused on grafting small cationic charged molecules with defined sizes onto surfaces of ZnO quantum dots that occurs without any further chemical procedures.

Accordingly, the ZnO quantum dots were synthesized in ethanol by hydrolysis of zinc acetate with lithium hydroxide. Figure 3 shows the XRD pattern of the dots that were aged for 4 h at 30 °C. All of the diffraction peaks are assigned to the standard hexagonal phase of ZnO with a wurtzite crystal structure, as reported in the JCPDS card (no. 36-1451, $a = 3.249$ Å, $c = 5.206$ Å). Importantly, no significant contributions from impurities arise in the XRD analysis. The widths of the XRD peaks confirm the nanocrystalline nature and the size of the ZnO nanocrystals. Figure 4a displays the absorption spectrum of the ZnO quantum dot ethanolic suspension with an absorption onset at 357 nm. From the absorption behavior, we have access to an estimation of the width of the particle size distribution (PSD). In particular, the ZnO nanoparticles are characterized by a narrow volume-weighted size distribution as represented in Figure 4b. This PSD was obtained via an algorithm developed by Segets et al.[63] Thereby the algorithm converts the measured absorption spectra into their single particle contributions using previously published work of Bergström[64] and Viswanatha et al.[65] From this PSD, a mean size of 4.5 nm was calculated coinciding with the average particles size obtained by XRD.

Achieving uniform and stable dispersions of particles is a key requisite for practical applications of colloidal ZnO nanoparticles. For example, mixing ZnO quantum dots with charged molecules is expected to form stable colloids with a narrow size distribution. To check the effect of the surface modification, the dispersibilities of **17**, **18**, **19**, and **20** grafted onto ZnO nanoparticles were compared to that of as-synthesized ZnO. To this end, the ZnO particles were simply mixed with **17**, **18**, **19**, and **20** in ethanol at 25 °C; see Experimental Section. Adsorption isotherms of the oligocationic molecules on the surface of the ZnO quantum dots are presented in Figure 5. The adsorption behavior follows a Langmuir isotherm for all four components. The highest experimental loadings of 0.97, 0.96, and 0.92 mg m^{-2} of the adsorbed **17**, **18**, and **19** molecules correspond to the maximum particle surface coverage of 0.98, 0.97, and 0.92 mg m^{-2}, respectively, which was estimated theoretically (Table 2). In case of **20**, the highest experimental coverage of only 0.56 mg m^{-2} is more than twice lower that the calculated maximum amount of 1.28 mg m^{-2} equivalent to a monolayer. These results indicate the insufficient adsorption of the largest oligocationic molecule.

Absorption spectra of ethanolic suspensions of ZnO recorded in the absence and in the presence of the oligocationic molecules are shown in Figure 6. The spectra were normalized with respect to the 336 nm peak, which corresponds to the absorption of the

(58) Hong, R. Y.; Chen, L. L.; Li, J. H.; Li, H. Z.; Zheng, Y.; Ding, J. *Polym. Adv. Technol.* **2007**, *18*, 901.
(59) Chibowski, S.; Paszkiewicz, M. *Adsorpt. Sci. Technol.* **2001**, *19*, 397.
(60) Liufu, S.; Xiao, H.; Li, Y. *Powder Technol.* **2004**, *145*, 20.
(61) Shim, J.-W.; Kim, J.-W.; Han, S.-H.; Chang, I.-S.; Kim, H.-K.; Kang, H.-H.; Lee, O.-S.; Suh, K.-D. *Colloids Surf., A* **2002**, *207*, 105.
(62) Xiong, H.-M.; Wang, Z.-D.; Liu, D.-P.; Chen, J.-S.; Wang, Y.-G.; Xia, Y.-Y. *Adv. Funct. Mater.* **2005**, *15*, 1751.
(63) Segets, D.; Gradl, J.; Taylor, R. K.; Vassilev, V.; Peukert, W. *ACS Nano* **2009**, *3*, 1703.
(64) Bergstrom, L.; Meurk, A.; Arwin, H.; Rowcliffe, D. J. *J. Am. Ceram. Soc.* **1996**, *79*, 339.
(65) Viswanatha, R.; Sapra, S.; Satpati, B.; Satyam, P. V.; Dev, B. N.; Sarma, D. D. *J. Mater. Chem.* **2004**, *14*, 661.

Scheme 5. Acidic Ether Cleavage and Final Quaternization Reaction To Obtain the Cationic Charged Target Molecules

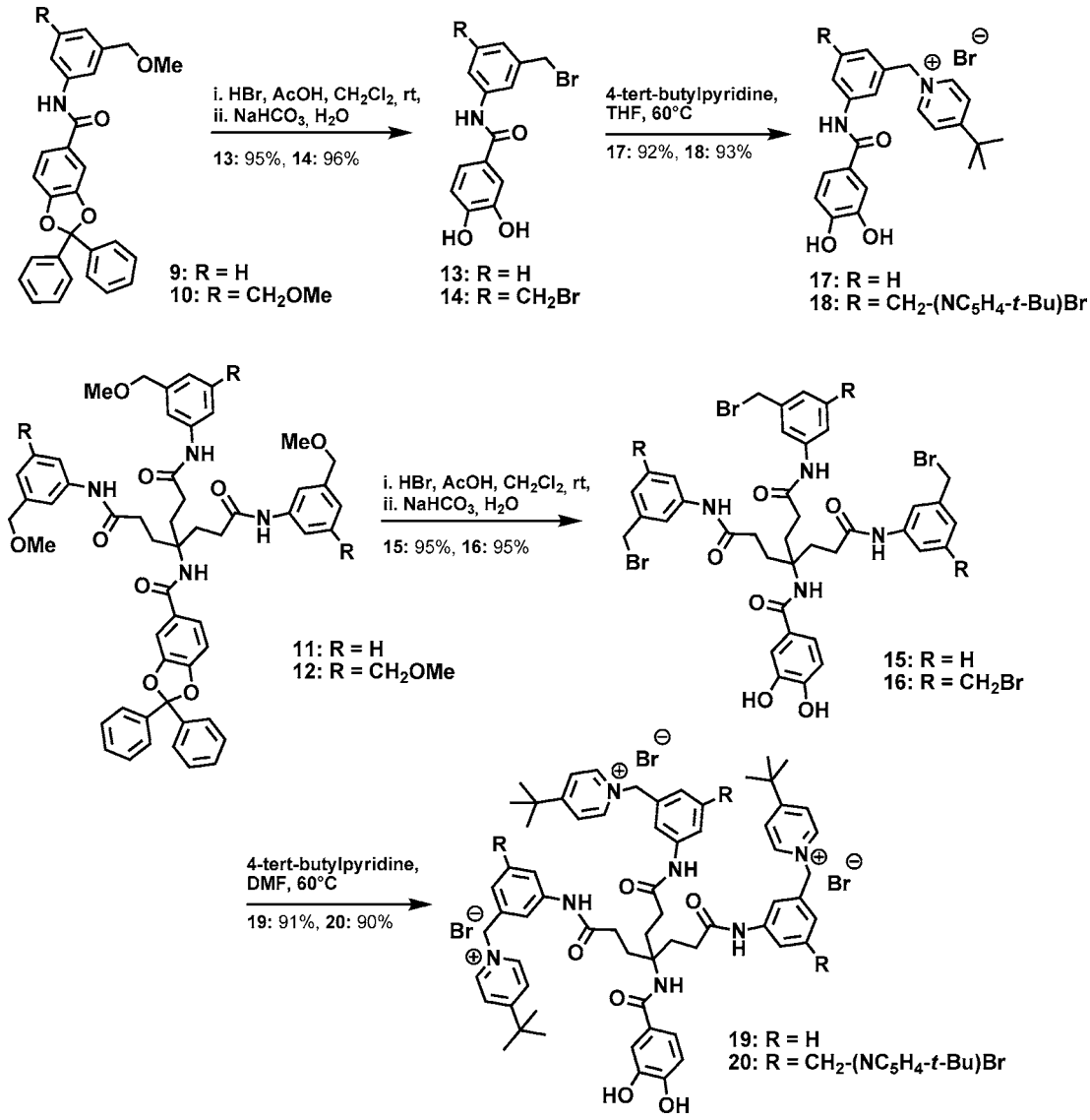

ZnO quantum dots. In addition, the features of **17**, **18**, **19**, and **20** (Figure 7) are also discernible. Two peaks at about 305 and 330 as well as a broad absorption with an onset at about 380 nm correspond to **17** and **18**, whereas the peak around 290 nm is a characteristic feature of **19** and **20**. It is interesting, however, that in the case of the ZnO quantum dots with **17**, **18**, and **19** (Figure 6) the absorption behaviors indicate that the particles are stable in suspension without noticeable aggregation. Thus, with a mean diameter below 10 nm clearly situated in the Rayleigh regime, they are too small to scatter light. When the diameter of particles increases due to their growth and/or aggregation, scattering occurs and the extinction at $\lambda > 364$ nm is nonzero.[65] In line with our previous observations,[8,66] the ZnO particle growth for particles exceeding a size of 12 nm is neglected. Thus, the only process that takes place in the suspensions is particle aggregation, which is the origin for scattering as observed in the case of **20** that is adsorbed onto ZnO surface (Figure 6). Transparent suspensions of **17**, **18**, and **19** (Figure 8) grafted onto ZnO surfaces were rapidly obtained after mixing the reactants. The corresponding suspensions remained stable at room temperature for several weeks. How-

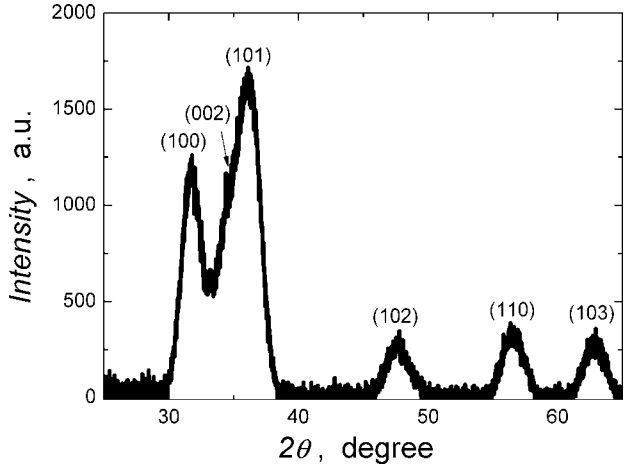

Figure 3. X-ray diffraction pattern of the ZnO nanoparticles aged at 30 °C for 4 h. All peaks correspond to the ZnO wurtzite crystal structure. The broadness of the XRD peaks reveals the nanocrystalline nature of the ZnO powders.

(66) Marczak, R.; Segets, D.; Voigt, M.; Peukert, W. *Adv. Powder Technol.* **2010**, *21*, 41.

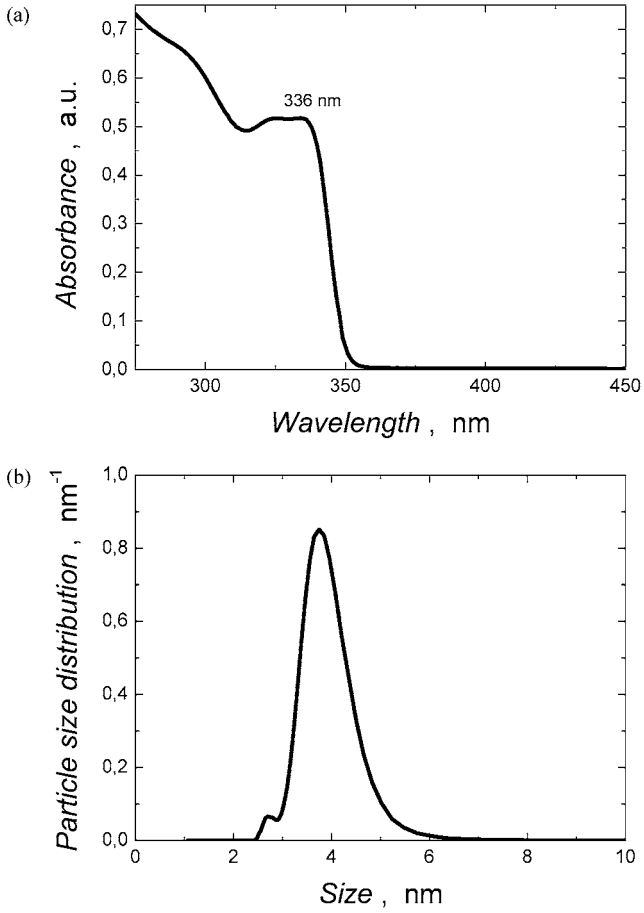

Figure 4. (a) Absorption spectra of the ZnO nanoparticles in ethanolic solution recorded after 4 h of aging at 30 °C. (b) Volume density distributions of the ZnO nanoparticles in ethanolic solution obtained by inversion of the UV−vis absorption spectrum (Figure 4a).

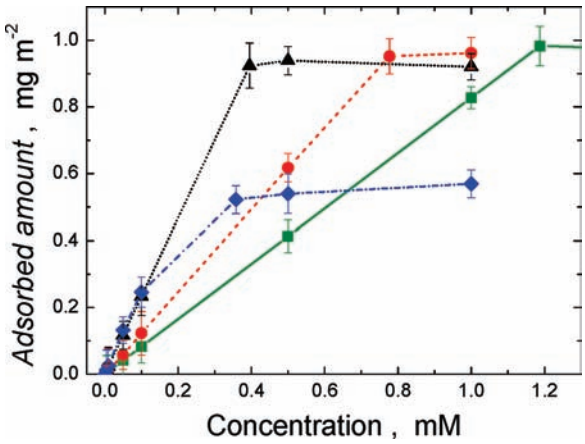

Figure 5. Adsorption isotherms of **17** (green ■ and line), **18** (red ● and line), **19** (▲ and line), and **20** (blue ◆ and line) on the surface of ZnO quantum dots at 25 °C.

ever, the suspension containing ZnO and **20** turned turbid, indicating that the ZnO nanoparticles are subject to significant aggregation (Figure 8).

To obtain quantitative information about the colloidal stability of the ZnO quantum dots grafted with the **17**, **18**, **19**, and **20**, zeta potential measurements were performed. In general, the absolute value of the zeta potential correlates with the colloidal stability due to electrostatic repulsions between particles. If

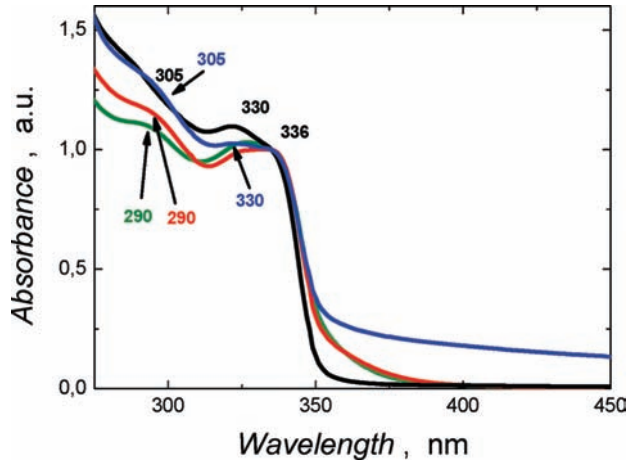

Figure 6. Normalized absorption spectra of **17** (green line), **18** (red line), **19** (black line), and **20** (blue line) adsorbed on the surface of ZnO quantum dots measured in ethanol at 25 °C.

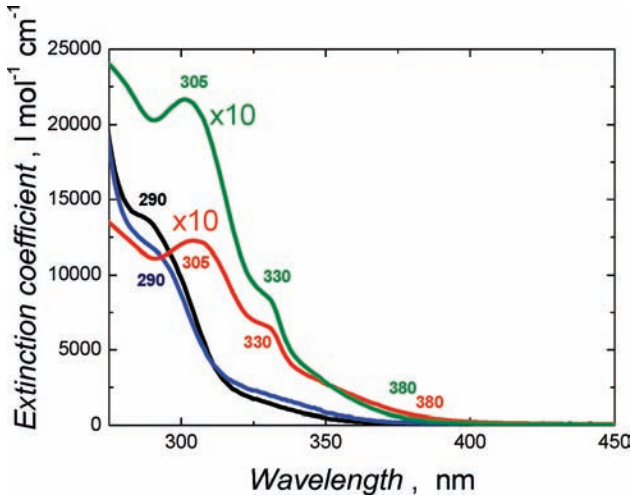

Figure 7. Extinction spectra of **17** (green line), **18** (red line), **19** (black line), and **20** (blue line) in ethanol at 25 °C.

particles have large negative or positive potentials, repulsion dominates without appreciable aggregation. However, if particles have low zeta potential values, the absence of repulsive forces gives way to aggregation.[67] Acetate groups, which originate from the precursor materials, are adsorbed on the surface and initially stabilize the ZnO nanoparticles. However, during the three times repeated washing steps, when the still unreacted reaction precursors (zinc acetate and lithium hydroxide) and the reaction byproduct (lithium acetate) are removed, the number of the protecting acetate groups is reduced. Therefore, in case of three times washed ZnO nanoparticles, the remaining amount of the acetate on the surface is unable to maintain sufficient stabilization against agglomeration of the ZnO nanoparticles in ethanol for longer than 30 min. Thus, zeta potentials of -8.9 ± 2.8 mV for the 0.05 M ethanolic suspensions of the ZnO quantum dots relate to the low stability of the corresponding suspension and a negative surface charge.

Figure 9 shows the zeta potential values of ZnO nanoparticles as a function of the concentration of various oligocationic molecules in ethanol. The absolute value of the zeta potential is influenced by the presence of both the remaining acetate

(67) Lagaly, G.; Schulz, O.; Zimehl, R. *Dispersionen und Emulsionen*; Steinkopff: Darmstadt, 1997.

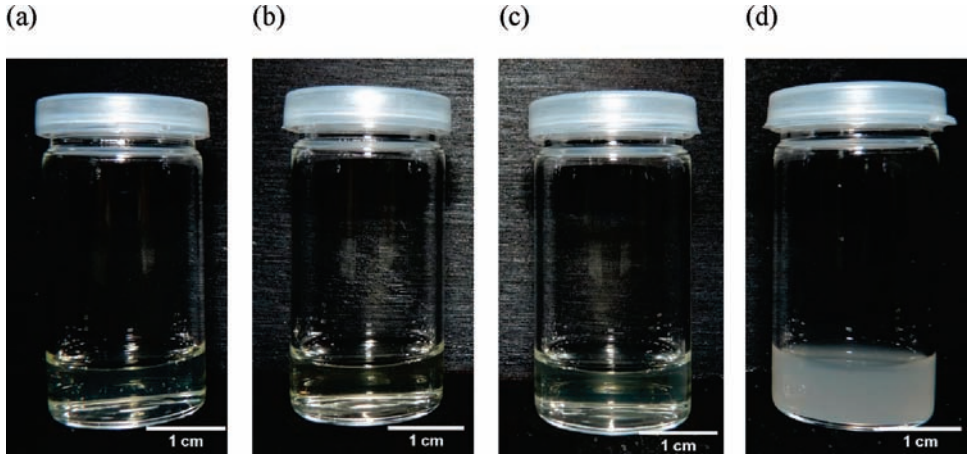

Figure 8. Visual observation of the stability of ZnO quantum dots grafted with **17** (a), **18** (b), **19** (c), and **20** (d) in ethanol at 25 °C.

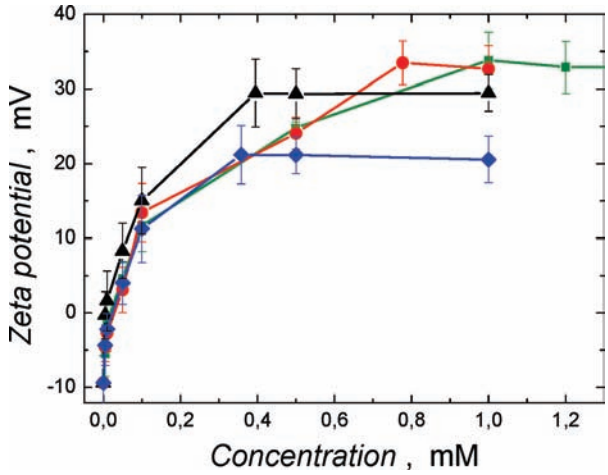

Figure 9. Zeta potential of ZnO quantum dots for different additives concentrations: **17** (green ■ and solid line), **18** (red ● and line), **19** (▲ and line), and **20** (blue ◆ and line).

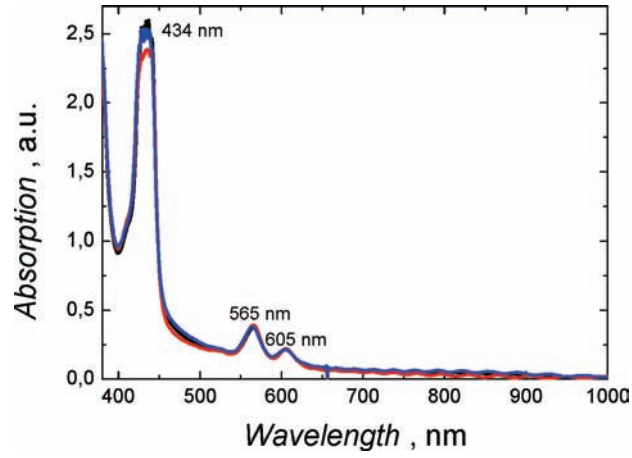

Figure 10. UV/vis absorption spectra of ZnO mesoporous films functionalized with **18** (red line), **19** (black line), and **20** (blue line) after sensitization with **21**.

groups as well as the grafted oligocationic molecules on the surface of the ZnO nanoparticles. In all cases, increasing zeta potential values were observed with increasing dendrimer concentrations, indicating the specific adsorption of the molecules onto the ZnO nanoparticles surface. The curves thus reflect the adsorption behavior of the dendrimer molecules (Figure 5). The initially low magnitude of the zeta potential values indicates weak colloidal stability of the suspensions. Further, the zeta potentials rise up to maximum values of $+33.8 \pm 3.7$ and $+32.6 \pm 3.1$ mV for **17** and **18**, respectively, at about 1×10^{-3} M. The increase of lower zeta potential values, which is up to $+29.5 \pm 3.3$ and $+21.2 \pm 2.5$ mV for **19** and **20**, respectively, at about 3.5×10^{-4} M was noted. When the concentrations of **17**, **18**, and **19** on the surface of the ZnO quantum dots increase, higher absolute zeta potentials give rise to stronger electrostatic repulsion between the particles. In stark contrast, low zeta potentials as they are obtained for different concentrations of **20** indicate that this molecule changes the sign of the surface charge but is unable to maintain the stability against agglomeration of the ZnO quantum dots in ethanol. The overall changes in stability are rationalized on the basis of the electrical double layer, which decreases, for example, toward the higher charge concentrations on the particle surface.

In general, changes in the colloidal stability as a function of the size and charge of the oligocationic molecules (**17**, **18**, **19**, and **20**) were observed during our experiments. The results show the enhanced stability after grafting the ZnO quantum dots with **17**, **18**, and **19**, while the stability is reduced after grafting with **20**.

Photophysical Characterization of DSSCs. Despite the aforementioned advantages in the control over morphology down to the nanoscale regime, there are only few examples utilizing supramolecular principles in solar cell construction and design.[3] Introducing the concept of noncovalent bonds (i.e., electrostatic interaction) in solar cells opens several interesting possibilities, for example, easy exchange of the absorbing species, introducing extra driving force via a charge gradient and the facile construction of multilayers. This is, to the best of our knowledge, the first example for utilizing structurally similar anchors bearing a different number of charges to influence the open circuit voltage (V_{oc}) systematically. In a proof of principle, the photophysical characterization (i.e., UV−vis absorption spectroscopy, incident photon to current efficiency (IPCE), and current voltage measurements) of a supramolecular DSSC is shown. The absorption spectra of ZnO films functionalized with **18**, **19**, or **20** and sensitized with zinc-5,15-bis-[2′,6′-bis-{2″,2″-bis-(carboxy)-ethyl}-methyl-4′-*tert*-butyl-pheny]-10,20-bis-(4′-tert-butylphenyl)porphyrin-octasodium-salt[6] **21** are gathered in Figure 10. There is no appreciable difference in the amount of dye adsorbed, leading us to the assumption that **18**, **19**, and **20** are all suitable for the stable electrostatic attachment of the dye.

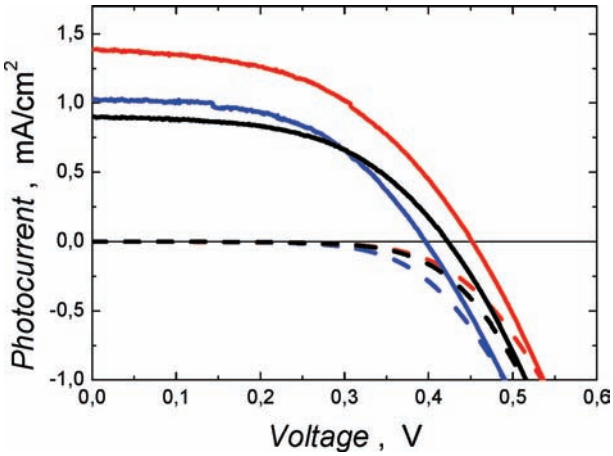

Figure 11. $I-V$ characteristics of DSSCs under AM1.5 illumination at 100 mW/cm^2 and in the dark (dashed lines), for ZnO electrodes grafted with **18** (red line), **19** (black line), and **20** (blue line) before dye sensitization.

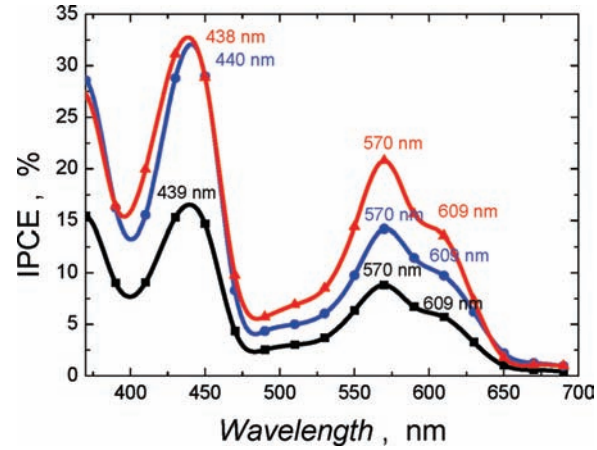

Figure 12. IPCE spectra of differently functionalized ZnO films sensitized with porphyrin, for ZnO electrodes grafted with **18** (red line), **19** (black line), and **20** (blue line) before dye sensitization.

Next, current voltage characteristics were recorded for the DSSCs (Figure 11). In terms of V_{oc}, a clear trend evolves, which suggests that the positive functionalization of the ZnO surface leads to decreased V_{oc}. Less concise is the trend for I_{sc}, although the values seem to decrease as well. All open circuit voltages are, as is typical for porphyrin sensitized solar cells, around 0.4 V with a maximum for the **18** functionalized ZnO film of 0.45 V. The maximum efficiency is at 0.31%, which is, taking the low overall absorption of the dye on the rather thin ZnO films into account, outstanding. It is difficult to compare this value to other systems due to the unique character of the supramolecular binding motif. It is, however, in the range of systems using porphyrins covalently bound to ZnO.[68] The results of the current voltage measurements are summarized in Table 1.

Table 1. Summary of Device Characteristics of DSSCs under AM1.5 Illumination at 100 mW/cm^2, for ZnO Electrodes Grafted with **18**, **19**, or **20** before Dye Sensitization

oligocationic molecule	I_{sc} (mA)	V_{oc} (V)	FF (%)	η (%)
18	1.39	0.45	63	0.31
19	0.9	0.42	38	0.20
20	1.02	0.40	52	0.21

Finally, in IPCE measurements (Figure 12), we confirmed that electron injection is indeed evolving from the dye, because the IPCE spectral overlap resembles the absorption features of the dye. The slight red-shift of the IPCE value can be attributed to down-conversion of higher energy photons due to scattering. The photon to current conversion efficiency is disproportionately favored in the region of the Q-band absorptions (i.e., 550−610 nm) when contrasted to that of the Soret band (i.e., around 430 nm) absorptions.

The electrostatic interaction is an efficient and versatile motif for the construction of DSSCs. With the permanently charged molecules synthesized, a stable interaction even in the high ionic strength environment of the electrolyte could be achieved between the mesoporous ZnO surface and the dye.

Experimental Section

Synthesis of ZnO Quantum Dots. All chemicals were analytical grade reagents used without further purification. ZnO quantum dots were prepared according to the procedures reported earlier.[8,66] Briefly, 1.09 g of zinc acetate dihydrate (ACS grade, 98.0%, VWR, Germany) was dissolved in 50 mL of boiling ethanol (99.98%, VWR, Germany) at atmospheric pressure and cooled to room temperature. Next, 0.17 g of lithium hydroxide (98%, VWR, Germany) was dissolved in 50 mL of boiling ethanol and also cooled to the synthesis temperature. Further, the lithium hydroxide solution was added dropwise to the cold zinc acetate solution under vigorous stirring. Immediately after synthesis, aging processes commence with an evolving particle diameter.[8,66] Next, after 4 h of aging at 30 °C, the ZnO nanoparticles were three times washed to remove the reaction byproduct lithium acetate by repeated flocculation affected by addition of *n*-heptane (Rotisolve HPLC, Carl Roth GmbH + Co. KG, Germany). White ZnO flocculates precipitated immediately after the addition of heptane. Afterward, the supernatant containing the lithium acetate was separated from the white ZnO precipitate by centrifugation at 3500 rpm for 10 min (Labofuge 400, Heraeus Instruments GmbH, Germany) and decantation. For colloidal characterization, the ZnO flocculates were redispersed in ethanol.

ZnO Quantum Dots Surface Functionalization. To examine the capability for the surface functionalization of the ZnO surface, three times washed ZnO quantum dots were mixed with a different amount of the oligocationic molecules in ethanol (concentrations from 5×10^{-6} to about 1×10^{-3} M). The mixture was sonicated for 15 min for the sake of adsorption. The mass of the adsorbed molecules on the surface of the ZnO nanoparticles was obtained from the difference of the initial amount of the molecules used for the suspensions preparation and the amount of the not adsorbed molecules. Thus, the suspensions of ZnO nanoparticles and different amount of the oligocationic macromolecules were centrifuged until the covered ZnO nanoparticles completely settled down. Next, the absorption spectra of the supernatants were measured at 25 °C to determine the amount of the not adsorbed molecules. The data were considered in terms of the mass of adsorbed oligocationic molecules per unit area of the ZnO quantum dots as a function of the total amount of molecules added to the suspension.

The surface of as-synthesized ZnO quantum dots is not bare, but acetate groups, which originate from the precursor materials, are adsorbed on the surface of the crystals.[8,66] The amount of the residual acetate of 10 wt % was determined by measuring the weight loss that occurred upon heating the sample in thermogravimetric analysis (TGA) (not shown).

Considering the particle size of 4.5 nm as calculated from the absorption spectrum (Figure 3a) by an algorithm developed by Segets et al.,[63] the total surface area of a ZnO nanoparticle was calculated to be 63.6 nm^2. Thus, the average number of the acetates after the third washing step was estimated to 5 molecules per nm^2

(68) Galoppini, E.; Rochford, J.; Chen, H.; Saraf, G.; Lu, Y.; Hagfeldt, A.; Boschloo, G. *J. Phys. Chem. B* **2006**, *110*, 16159.

and is equivalent to 43% of a monolayer.[66] Therefore, just 57% (36.3 nm^2) of the particle surface could be grafted with the oligocationic molecules.

Additionally, the average surface areas have been optimized theoretically in a vacuum and using an implicit solvent environment in MeOH and H_2O within the semiempirical MO-theory using the AM1 Hamiltonian. From the optimized geometries, the surface areas, which are shown in Table 2, have been computed according to the formula for triangular surfaces. Thus, to form a monolayer, the maximal number of the adsorbed molecules per nanoparticle,[66] concentrations of the oligocationic molecules required to completely cover the ZnO surface in a 0.05 M ethanolic suspensions, and the maximal amount of the molecules adsorbed on the total particles surface could be estimated. All of the values are summarized in Table 2.

Table 2. Properties of the Oligocationic Molecules Adsorbed on the ZnO Quantum Dots Surface

oligocationic molecule	average surface, nm^2	max. number of adsorbed molecules	concentration required to form a monolayer, mol L^{-1}	max. adsorbed amount, mg m^{-2}
17	0.77	47	11.8×10^{-4}	0.98
18	1.18	30	7.8×10^{-4}	0.97
19	2.32	15	3.9×10^{-4}	0.93
20	2.56	14	3.6×10^{-4}	1.28

Characterization of ZnO Nanoparticles. Optical properties of the ZnO nanoparticles were determined from UV−vis absorption spectra recorded at 25 °C using a Cary 100 Scan UV−visible spectrophotometer (Varian Deutschland GmbH, Germany) with a cuvette of 10 mm optical path length. The zeta potentials of 0.05 mol L^{-1} ZnO ethanolic suspensions (with respect to the Zn^{2+} concentration) were obtained at 25 °C via dynamic light scattering (DLS) by using a Malvern Nano ZS Instrument (Malvern Instruments GmbH, Germany) using laser Doppler electrophoresis. Structural analysis of the ZnO nanoparticles was performed with a D8 Advance (Bruker AXS, Germany) X-ray diffractometer (XRD) in the Bragg−Brentano geometry using Cu Kα radiation ($\lambda = 0.154$ nm). The XRD patterns were recorded in the range of 2θ from 20° to 70°.

Device Fabrication. The ZnO nanoparticles suitable to be used in a dye-sensitized solar cell were prepared by dissolving 7.8 g of zinc acetate dihydrate (ACS grade, 98.0%, VWR, Germany) in 43.6 mL of methanol (99.9%, Carl Roth GmbH & Co KG, Germany). Next, ZnO was precipitated by adding tetramethylammonium hydroxide (25% (w/w) in methanol, Sigma-Aldrich, Germany). The reaction mixture was stirred for 3 h at 75 °C under refluxing. During this time, flocculation of the nanoparticles was observed. To remove the remaining salts, the ZnO flocculates were centrifuged. The supernatant was removed by decantation, and the ZnO flocculates were washed with ethanol. The particles were redispersed by sonication for 15 min.

ZnO paste was fabricated by mixing the obtained nanoparticles with 10% ethanolic solutions of ethyl cellulose (5−15 mPa and 30−50 mPa, Aldrich) in a 1:1 ratio. The resulting transparent paste was doctor bladed onto TEC 15 F/SnO_2 conducting glass substrates utilizing two layers of Scotch magic tape (approximately 100 μm) as spacer. After evaporation of the solvent, the films were calcinated at 450 °C, yielding transparent mesoporous films of 4 μm thickness. The films were then immersed in 10^{-4} M ethanolic solutions of **18**, **19**, and **20** overnight. Afterward, the films were rinsed with ethanol and dried in a stream of nitrogen. The functionalized films where then immersed in a 10^{-5} M aqueous solution of zinc-5,15-bis-[2′,6′-bis-{2″,2″-bis-(carboxy)-ethyl}-methyl-4′-*tert*-butyl-pheny]-10,20-bis-(4′-*tert*-butylphenyl)porphyrin-octasodium-salt[2] for 4 days to guarantee efficient attachment and ion exchange.

DSSCs have been fabricated from these slides. For counter electrode fabrication, uncoated conducting glass slides were cut into pieces, and holes of 1 mm^2 were drilled at the edge of the active area. A thin film of H_2PtCl_6 (0.01 M in ethanol) was spread over the conducting glass electrode, which was allowed to dry in air prior to firing at 380 °C for 20 min. The ZnO and platinum counter electrode was then sealed together with a transparent film of Surlyn 1472 (Dupont) cut as a frame around the nanocrystalline ZnO film. A solution of 0.6 M 1-methyl-3-propylimidazolium iodide (MPII), 0.03 M I_2 in methoxyacetonitrile, was employed as electrolyte. The electrolyte was introduced through a hole drilled in the counter electrode and immediately sealed.

Conclusions

In short, advanced inorganic nanostructures via stable attachment of cationically charged monolayers onto ZnO nanoparticles, and solid-state mesoporous ZnO surfaces were realized. Remarkable improvement in colloidal stability ensured the integration into photovoltaic devices. The key to our approach was a novel synthetic route generating highly reactive benzylic bromides, which react readily with nucleophiles like pyridine resulting in quarternized N-atoms and generating permanent cationic charges in very high yields and very good purity. 3-Methoxymethylaniline and 3,5-bis(methoxymethyl)aniline were successfully connected to carboxylic acid containing building blocks and transformed quantitatively into the corresponding benzylic bromides by means of hydrobromic acid. The cationic charges are obtained by the reaction with 4-*tert*-butylpyridine leading to the quantitative formation of cationic charges. In addition to the cationic functionality, these dendritic systems are equipped with a catechol anchoring group, which forms a very strong covalent bond to ZnO nanostructures. A distinctive factor of this approach is that once the molecules are attached to the surface, a chemical post-treatment is not necessary anymore delivering high homogeneity of the mono molecularly surface layer of **17**, **18**, **19**, and **20**. Importantly, changes in the colloidal stability of the ZnO nanoparticles grafted with the cationic dendric molecules were observed and directly linked to the size and charge of the attached molecules. Greatly enhanced stability after grafting the ZnO quantum dots with **17**, **18**, and **19** is shown, while the stability is reduced after grafting with **20**. Motivated by these results, the successful integration of molecularly modified mesoporous ZnO nanostructures into a DSSC device has been demonstrated in a proof of principle experiment. The advanced design of the molecules allows stable attachment of oppositely charged porphyrins via an LbL approach even in the high ionic strength environment of an electrolyte commonly utilized in DSSC systems. The relatively high efficiencies in regard to ZnO and porphyrin-based DSSCs were explained by the build-in driving force provided by the positive charge of the polyions. These already very promising results (i.e., efficiencies of up to 0.31%) are expected to be greatly enhanced by the utilization of dye multilayers. Thus, by this approach, the complementary spectral properties of various dyes can be utilized, and even a built-in redox gradient can further enhance the efficiency.

Acknowledgment. We gratefully acknowledge the funding of the German Research Council (DFG), which, within the framework of its "Excellence Initiative", supports the Cluster of Excellence "Engineering of Advanced Materials" at the University of Erlangen-Nuremberg. We are grateful to Prof. R. N. Klupp Taylor for comments and discussion. We dedicate this article to Eiichi Nakamura on the occasion of his 60th birthday.

Supporting Information Available: Detailed synthetic procedures and spectroscopic data for all new compounds. This material is available free of charge via the Internet at http://pubs.acs.org.

JA106076H